


# Multifocal bone and bone marrow lesions in children — MRI findings

Maria Raissaki<sup>1</sup>  · Stelios Demetriou<sup>1</sup> · Konstantinos Spanakis<sup>1</sup> · Christos Skiadas<sup>1</sup> · Nikolaos Katzilakis<sup>2</sup> · Emmanouil G. Velivassakis<sup>3</sup> · Eftichia Stiakaki<sup>2</sup> · Apostolos H. Karantanas<sup>1</sup>

Received: 6 June 2016 / Revised: 13 September 2016 / Accepted: 18 October 2016 / Published online: 21 December 2016  
© Springer-Verlag Berlin Heidelberg 2016

**Abstract** Polyostotic bone and bone marrow lesions in children may be due to various disorders. Radiographically, lytic lesions may become apparent after loss of more than 50% of the bone mineral content. Scintigraphy requires osteoblastic activity and is not specific. MRI may significantly contribute to the correct diagnosis and management. Accurate interpretation of MRI examinations requires understanding of the normal conversion pattern of bone marrow in childhood and of the appearances of red marrow rests and hyperplasia. Differential diagnosis is wide: Malignancies include metastases, multifocal primary sarcomas and hematological diseases. Benign entities include benign tumors and tumor-like lesions, histiocytosis, infectious and inflammatory diseases, multiple stress fractures/reactions and bone infarcts/ischemia.

**Keywords** Bone · Bone marrow · Children · Developmental disease · Magnetic resonance imaging · Multifocal · Neoplasms · Polyostotic

## Introduction

Magnetic resonance imaging (MRI), including whole-body MRI, has been increasingly employed for the detection, characterization and follow-up of bone marrow lesions in children with diseases and conditions that may potentially affect the bones or bone marrow [1]. The interpretation of findings may prove particularly difficult because of the prominence of red bone marrow in children and because most lesions exhibit a nonspecific pattern of low intensity on T1-W sequences and high intensity on T2-W sequences [1]. Multifocality of symptomatic lesions is not uncommon. Occasionally, these are found incidentally in a scan performed for the investigation of abdominal or thoracic pathology and may even go unnoticed. The radiologist will be asked to appreciate all lesions, provide a differential diagnosis and differentiate incidentalomas and benign lesions requiring conservative therapy or follow-up from potentially malignant lesions that require further investigation with blood smears, bone marrow aspirates or targeted biopsy. However, the diagnosis is rarely made based on MRI findings alone and is usually the result of the combination of clinical information, duration of symptoms, laboratory data, and radiographic, scintigraphic, PET-CT and CT appearances, when available. Occasionally, the diagnosis will be based on the evolution of clinical and imaging appearances.

Knowledge of the normal conversion pattern of bone marrow in childhood and of the spectrum of conditions that may cause multifocal bone and bone marrow lesions in children may aid in decision-making and appropriate management. This pictorial essay illustrates the appearances with conventional MRI sequences of conditions that cause multiple lesions in the same or different bones.

---

✉ Maria Raissaki  
mraissaki@yahoo.gr

<sup>1</sup> Department of Radiology, University Hospital of Heraklion, University of Crete, Faculty of Medicine, Heraklion, Crete, Greece

<sup>2</sup> Department of Pediatric Hematology-Oncology, University Hospital of Heraklion, University of Crete, Faculty of Medicine, Heraklion, Crete, Greece

<sup>3</sup> Orthopedic Clinic, University Hospital of Heraklion, Heraklion, Crete, Greece

## MRI technique

Selection of sequences type and planes in pediatric musculoskeletal MRI and in whole-body MRI is determined by the clinical indication. Whenever the main target tissue is bone marrow, baseline sequences include short-tau inversion recovery (STIR) or turbo spin-echo (TSE) proton density T2-W sequences with fat saturation in coronal only or in coronal and sagittal planes and T1-W sequences in the same planes. The sagittal plane is particularly useful for spinal and sternal foci. STIR and T1-W sequences are the two key pulse sequences used for whole-body MRI, while in some centers only STIR sequences are utilized [2, 3]. Axial sequences are time-consuming and are generally avoided whenever possible, especially in whole-body MRI.

The STIR technique is preferred because of its greater signal homogeneity and higher sensitivity for detecting lesions as compared with fat-suppressed proton density T2 TSE sequences, due to suppression of stationary tissue and not only fat tissue [3, 4]; its limitations include a lower signal-to-noise ratio and a longer scan time. Osteoblastic low signal intensity metastases may be missed with a water-sensitive sequence and a complementary T1-W sequence is obligatory in osteosarcoma patients.

T1-W sequences can be obtained as spin echo, fast/turbo spin echo or gradient echo. Gradient-echo sequences are faster, but their sensitivity and contrast resolution are lower because bone trabeculae are more conspicuous and the fatty component is obscured [2, 4].

Diffusion weighted imaging (DWI) and whole-body DWI with body background suppression (DWIBS) have been increasingly employed in musculoskeletal pediatric radiology [5–7]. It should be emphasized that restricted diffusion is a normal finding in the pelvis and lumbar spine in children and that an asymmetrical distribution seen in up to 48% of normal children should not be misinterpreted as abnormality [8].

The Dixon technique generates the following four sets of images with different image contrasts from a single acquisition: fat-only, water-only, in-phase and opposed-phase images. Water-only images offer almost perfect fat suppression. Marrow-replacing lesions can be distinguished from red marrow and other non-marrow-replacing conditions by detecting the absence of significant signal drop on opposed-phase images compared to in-phase images. As a result, this pulse sequence with multiple image contrast can be used to enhance lesion detectability on pre- and post-contrast whole-body MRI [2, 9]. Consequently, chemical shift or opposed-phase imaging either alone or in the context of Dixon technique may help differentiate true marrow lesions from normal red marrow.

## Normal age-related MRI findings

Bone marrow consists of red marrow, yellow marrow and supporting trabeculae. Red or hematopoietic marrow is hypervascularized, almost 100% cellular at birth and composed of precursors and mature red blood cells, white blood cells, megakaryocytes, platelets and supporting stroma. By adulthood, red marrow contains approximately 40% water, 40% fat and 20% protein. Yellow or fatty marrow has fewer red marrow elements, a larger amount of fat cells, is poorly vascularized and contains approximately 15% water, 80% fat and 5% protein by adulthood [10].

Bone marrow composition varies greatly with age and anatomical location within the skeleton [11–13]. Normal conversion of red marrow to yellow marrow starts during the neonatal period and occurs in a predictable and progressive manner, from the appendicular to the axial skeleton, from the distal to the proximal parts of each bone, from the diaphysis to the metaphysis and from central to endosteal, in a bilateral symmetrical fashion (Fig. 1) [10, 13, 14].

Signal intensity on MRI largely depends on the proportion of fat in the marrow. Red marrow follows the signal intensity of muscle and exhibits intermediately low signal intensity on T1-W and T2-W images at birth [15]. During childhood, red marrow exhibits progressive loss of cellularity and its signal intensity becomes equal or slightly greater than muscle on T1-W, and higher than muscle on T2-W and STIR sequences.

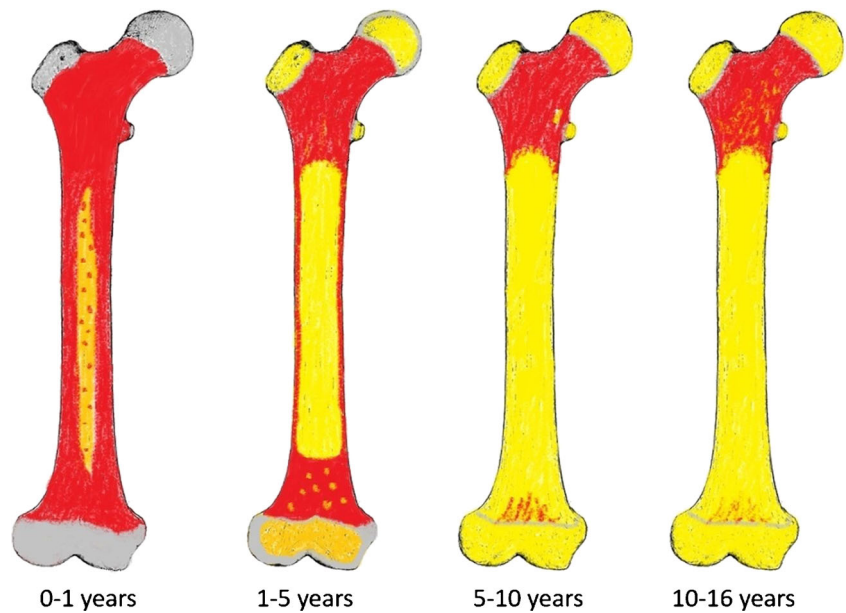
Yellow marrow follows the signal intensity of subcutaneous fat and exhibits relatively high signal intensity on T1-W and T2-W images and low signal intensity on STIR images compared to muscle and red marrow.

At birth, nearly the entire osseous skeleton is composed of red marrow (Fig. 2). In children older than 1 year, epiphyses and apophyses contain yellow marrow. As age progresses, red marrow areas remain at the proximal metaphyses of long bones and in the axial skeleton (Figs. 3 and 4), [11, 13, 15]. The short bones of the feet may contain stippled areas of abnormal signal attributed to red marrow rests or altered biomechanics (Fig. 5) [16]. Red marrow exhibits greater signal decrease on opposed-phase gradient echo sequences (Fig. 6), faint gadolinium enhancement and greater apparent diffusion coefficient values compared to yellow marrow.

## Bone marrow reconversion

Yellow marrow may reconvert to red marrow following increased demand for hematopoiesis. These conditions

**Fig. 1** Schematic representation of bone marrow conversion. At birth, epiphyses are cartilaginous (*grey*) and the bone marrow is almost exclusively red (*red*), with narrow central diaphyseal areas of yellow marrow (*yellow*). The epiphyses gradually contain yellow marrow. With conversion progression, the distal metaphyses and wider central diaphyseal areas convert first whereas the proximal metaphyses and metaphyseal equivalent sites convert last. (Modified from [2])



mainly comprise chronic hemolytic anemias (Fig. 7), treatment with hematopoietic growth factors, increased oxygen demands (high altitude residence), impaired oxygen delivery (cyanotic congenital heart diseases) and, rarely, menorrhagia or intense athletic activity (long-distance running) in adolescents [15]. Reconversion

occurs in the reverse order of normal marrow conversion [15].

Special attention should be paid to children treated with hematopoietic growth factors (like G-CSF,

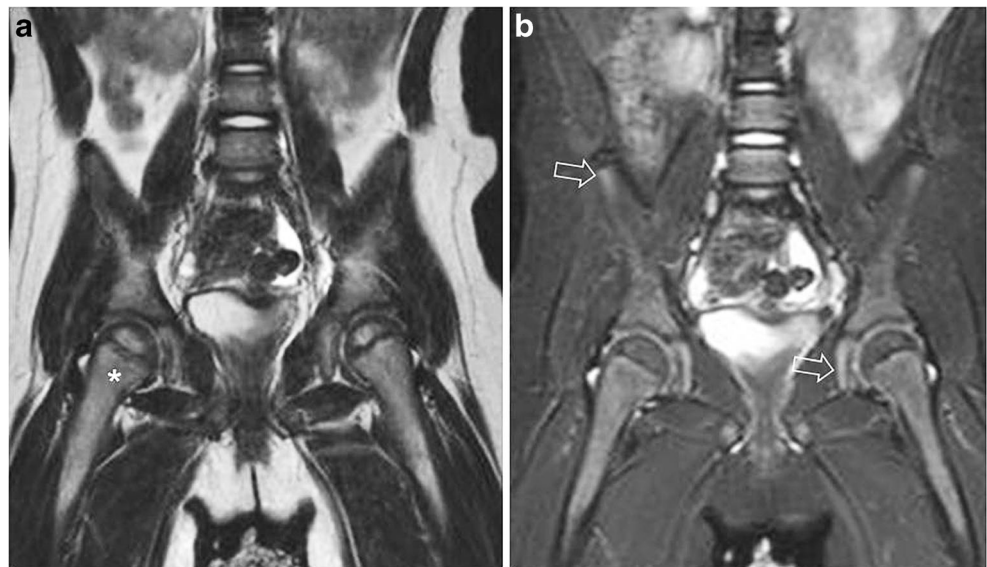


**Fig. 2** MRI of a newborn boy scanned for lipomeningocele (not shown). Sagittal T1-weighted MRI (TR/TE: 500/11 ms). Note signal similarity between cellular red bone marrow (\*), paraspinal muscles (m) and intervertebral discs (*arrow*)



**Fig. 3** MRI of the spine in a 9-year-old-girl. Sagittal T1-weighted MR image (TR/TE: 500/11 ms). Predominance of red marrow at the end plates (*arrow*) and central perivascular location of yellow marrow (\*) reflects the conversion pattern from central to endosteal. Note the preservation of intervertebral disc, muscle and red marrow isointensity

**Fig. 4** Normal bone marrow in a 2-year-old boy. Red marrow predominates at the proximal femoral metaphyses and vertebral end plates. **a** Coronal T2-weighted MR image (TR/TE: 300/120 ms). The red marrow signal intensity at metaphyses (\*) is lower than that of yellow marrow at epiphyses and diaphyses and higher than that of muscles due to progressive loss of cellularity. **b** Coronal short tau inversion recovery MRI (TR/TE/TI: 3,500/43/150 ms). Fatty marrow exhibits signal hypointensity at the femoral epiphyses whereas red marrow at the end plates and metaphyseal-equivalent areas of the pelvis (arrows) is slightly hyperintense compared to muscles



granulocyte-macrophage colony-stimulating factor and erythropoietin). In these children, foci of bone marrow reconversion may simulate diffuse marrow involvement or metastases on MRI (Fig. 8), develop within a few weeks following initiation of therapy and coincide temporally with increases in neutrophil counts [17].

As a rule of thumb, bone marrow in children older than 1 year on T1-W sequences should exhibit signal intensity similar or higher compared to neighboring intervertebral discs or hyaline cartilage [11, 15]. A neonatal pattern of bone marrow should not be interpreted as normal in older children.

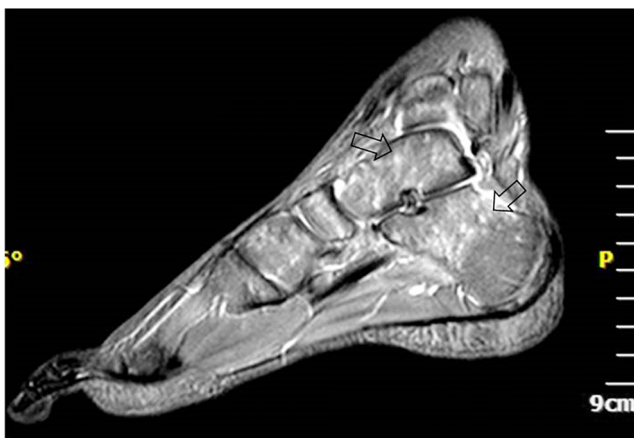


**Fig. 5** MRI of the ankle in an 11-year-old female ballet dancer with a stress reaction at the 3<sup>rd</sup> metatarsal (not shown). Sagittal short tau inversion recovery MRI (TR/TE/TI: 3,500/43/150/ ms). There are multiple dots and small areas of high signal (arrows) thought to represent asymptomatic red marrow rests. The same areas were hypointense at T1-weighted MR images

## Malignant conditions

### Metastases

Metastases to bone are usually hematogenous and asymptomatic unless there is cortical disruption. The most common primary tumors in children include neuroblastoma, leukemia/lymphoma, clear cell sarcoma, rhabdomyosarcoma, retinoblastoma, osteosarcoma and Ewing sarcoma [18].

The distribution of hematogenous skeletal metastases simulates the distribution of red marrow due to its increased blood supply. Metastases cause replacement of normal cells by neoplastic cells and appear as nonspecific focal circumscribed lesions, hypointense on T1-W and variably hyperintense on T2-W sequences. Metastases can be widespread and expansile (Fig. 9). Whole-body MRI has a higher sensitivity than skeletal scintigraphy for the detection of bone marrow metastases but a lower sensitivity than FDG PET [3, 19]. MR characteristics that have significant associations with metastases in neuroblastoma patients older than 12 months include homogeneous low T1 signal intensity, homogeneous high STIR signal intensity and a heterogeneous enhancement pattern on postcontrast T1-W sequences [20].

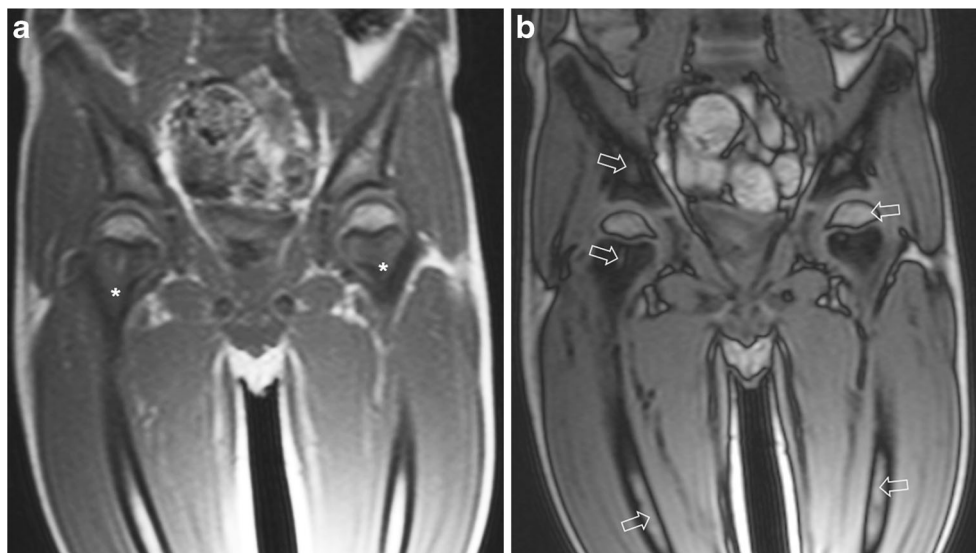
### Hematological malignancies

**Leukemia** is the most commonly encountered cancer in children younger than 15 years with acute lymphoblastic leukemia (ALL) being the most common type affecting children ages 2-5 years. Peripheral blood smears and/or bone marrow biopsy usually suffice to establish diagnosis.

Leukemia should be suspected in any child with anemia not associated with bleeding, associated or not with pallor,



**Fig. 6** MRI of the pelvis in a 7-year-old boy admitted for limping, left hip pain and leukocytosis. Final diagnosis was toxic synovitis. **a** Coronal fast low angle shot (FLASH) 2-D T1-W in-phase MRI (TR/TE/flip angle: 100 ms/5 ms/90°). Low signal intensity due to red marrow predominates at femoral metaphyses (\*). **b** Coronal FLASH 2-D T1-W out-of-phase MR image (100 ms/2 ms/90°). There is significant signal drop by 82% at the pelvis and femoral metaphyses and less at the femoral diaphysis due to coexistence of red marrow cells with few fatty cells. Fatty marrow areas including fatty islands fail to reduce signal intensity (arrows)



visceromegaly and complete blood count (CBC) with anemia and/or neutropenia (sometimes leukocytosis), or bone pain not associated with trauma with CBC with cytopenia [21]. Bone

pain due to leukemic marrow infiltration occurs in 30% of children with ALL and may simulate an infectious, rheumatological or orthopedic disorder, occasionally resulting in delayed diagnosis [22].

Radiographs may be normal or exhibit osteopenia ranging from mild forms to juxtaphyseal radiolucent metaphyseal bands. Osteosclerotic lesions are considered bone marrow infarcts at presentation or may be due to leukemic cell infiltration [22]. On MRI, leukemia may be seen as a neonatal type marrow in an older child or adult (Fig. 10) [22, 23]. Other patterns include diffuse nonuniform and patchy involvement [23]. Multifocal areas of leukemic infiltration tend to be large and with a predilection around the growth plates, occasionally with epiphyseal involvement. Periostitis, effacement of fatty marrow, and adjacent soft-tissue edema favor leukemia over hematopoietic red marrow [22, 24]. Smaller lesions are seen in relapse cases. During follow-up, bone marrow with abnormal signal intensity carries a differential diagnosis between leukemia relapse, marrow hyperplasia from G-CSF administration, osteonecrosis and stress injury related to osteopenia [24].

**Primary bone lymphoma** is rare and constitutes 4% of pediatric Non-Hodgkin type in children. The majority of cases are subtypes of diffuse large B-cell lymphoma with a more favorable prognosis compared to that of adults [25]. Bone involvement usually coexists with nodal lymphoma in stage IV lymphoma. Symptoms include localized pain and pathological fractures.

Abnormal aspects include lytic or mixed density lesions with a permeative pattern, periosteal reaction, eventual cortical destruction, a soft-tissue mass or a diffuse increase in opacity (“ivory” appearance) in plain films and CT scans, corresponding to lesions with low signal on T1-W and variable signal on STIR sequences (Fig. 11) [26, 27].

Bone marrow involvement in stage IV lymphoma may be focal or multifocal and may be missed at blind

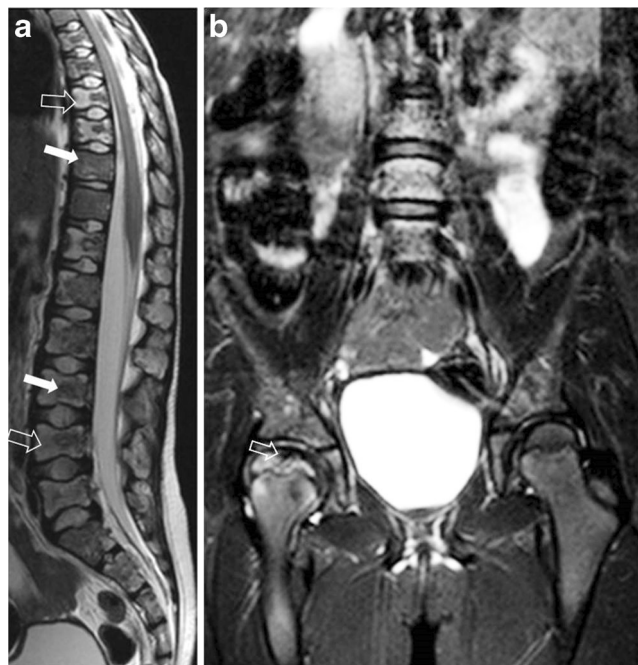


**Fig. 7** MRI of the spine and pelvis in a 7-year-old girl admitted for abdominal and right hip pain. Final diagnosis was double mutation for sickle cell anaemia, undiagnosed prior to hospitalization. **a** Sagittal T2-weighted MRI (TR/TE: 3,300/120 ms). Alternating hypointense and hyperintense bone marrow areas are considered to represent the combination of hyperplastic red marrow (solid arrows) and bone marrow edema due to acute micro infarctions (open arrows), respectively. **b** Coronal short tau inversion recovery MRI (TR/TE/TI: 3,500/43/150 ms). There is high signal intensity indicative of bone marrow edema at the flattened right femoral head, around a hypointense low signal area of subchondral fracture (arrow), indicative of avascular necrosis

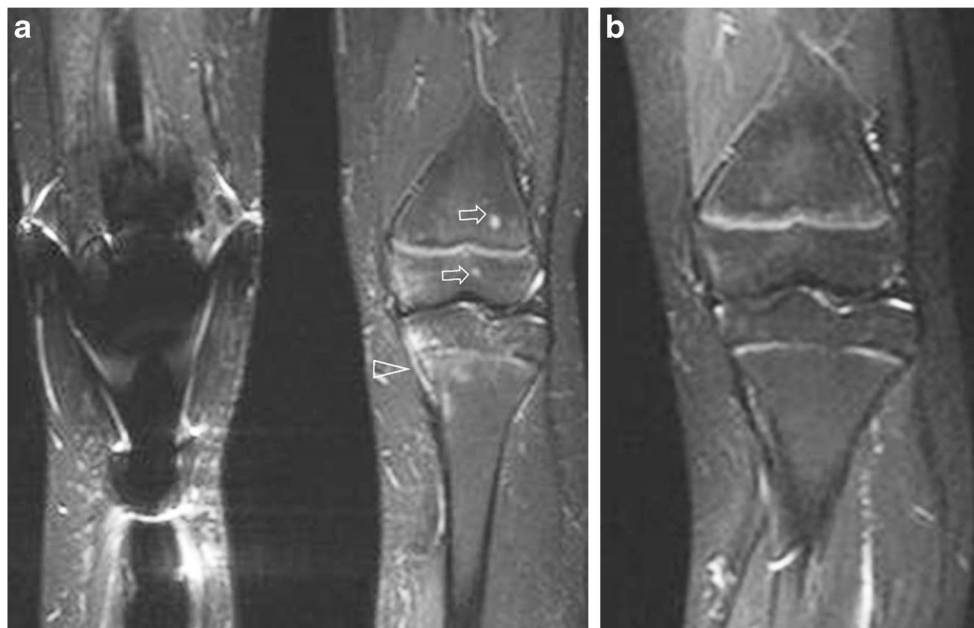


**Fig. 8** Follow-up MR Images of a 6-year-old boy treated for osteosarcoma of the right tibia. **a** Coronal short tau inversion recovery MRI (TR/TE/TI: 3,500/43/150 ms) of both knees postoperatively and following granulocyte colony stimulating factor treatment. There are high intensity foci around the left knee (arrows) with a differential diagnosis between hyperplastic bone marrow and metastatic lesions. Confluent hyperintensities around the

proximal tibial metaphysis (arrowhead) could be attributed to stress injury or marrow hyperplasia. **b** Coronal short tau inversion recovery MRI (TR/TE/TI: 3,500/43/150 ms) 6 months later and without any treatment. Lesions have resolved. Clinical correlation with the timing of therapy was necessary to make the differential diagnosis

biopsy. STIR whole-body MRI is more sensitive than conventional imaging in detecting high-intensity bone marrow involvement at initial staging; however, it

cannot differentiate residual and therapy-induced bone marrow signal abnormalities from new lymphomatous involvement [28].

**Fig. 9** Metastatic neuroblastoma in a 3-year-old boy. **a** Coronal short tau inversion recovery MRI (TR/TE/TI: 3,500/43/150 ms) at diagnosis. The primary tumor is situated at the left adrenal (\*). Note diffusely inhomogeneous bone marrow signal at the spine as well as the expansile nature of the right iliac wing metastasis (arrow). **b** Coronal T1-weighted MRI (TR/TE: 500/11) following 4 cycles of chemotherapy. Metastases cause large areas of sharply delineated hypointense marrow (arrows) compared to muscle and intervertebral discs



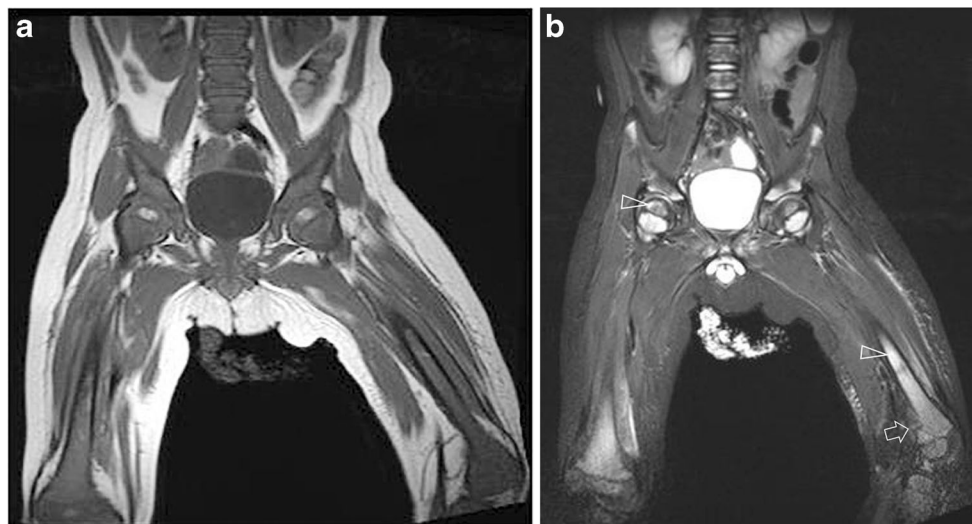


**Fig. 10** MRI of a 3-year old boy with persisting pain over a left knee fracture that turned out to be caused by acute lymphoblastic leukemia. **a** Coronal T1-weighted MRI (TR/TE: 500/11) through the hips. There is diffuse hypointensity in all imaged bones, including parts of the epiphyses, an appearance highly suggestive of a diffuse bone marrow

process when seen in a child older than 2 years of age. Symmetry should not be mistaken for normality. **b** Coronal short tau inversion recovery MRI (TR/TE/TI: 3,500/43/150 ms) through the hips. Diaphyseal and epiphyseal (arrowheads) involvement is confirmed. Note the healed left femoral fracture (arrow)

### Multifocal osteosarcoma

Osteosarcoma is the most common primary malignant osseous sarcoma in children and adults and may arise from malignant osteoid or bone-forming mesenchymal cells. Osteosarcoma can occur as a primary lesion or secondary to radiation therapy, bone infarct or chronic osteomyelitis. Osteosarcoma can present as a solitary lesion or, rarely, as multifocal disease with synchronous (within 6 months) or metachronous (more than 6 months apart) lesions [29, 30].

Osteosarcoma has a variable imaging appearance ranging from a pure lytic to a heavily ossified or a mixed lytic and blastic lesion. Cortical breakthrough and an aggressive periosteal reaction with Codman triangles or a “sunburst” appearance are often seen along with a soft-tissue mass. There might be a dominant large lesion whereas secondary osseous foci are smaller, occasionally sclerotic, well-defined, and without cortical disruption or periosteal reaction (Fig. 12).

### Multifocal Ewing sarcoma

Ewing sarcoma is the second most common primary malignancy of bones in children and accounts approximately for 3% of all pediatric cancers [29]. Presentation occurs mostly during the first 3 decades of life, especially between ages 4 and 25 years (95% of cases). Patients present with local pain and occasionally with a palpable soft-tissue mass [31].

Radiographic characteristics include an aggressive-looking lesion with a permeative lytic pattern and malignant periosteal reaction with an “onion ring” appearance. On MRI, lesions appear as low to intermediate signal on T1-W and

heterogeneously high signal on T2-W images. Occasionally, there are skip lesions proximally at the same bone [31]. There is rarely simultaneous involvement of multiple bones at presentation, called primary disseminated multifocal Ewing sarcoma (Fig. 13) [32].

Consequently, whenever a primary bone tumor is suspected radiographically, MRI should scan the entire involved bone, including adjacent joints and soft tissues to record the local extent of the tumor. F<sup>18</sup> FDG-PET has the highest specificity and sensitivity for assessment of bone and bone marrow metastases and, if positive, light microscopy of bone marrow aspirates and biopsies taken at sites distant from the primary tumor are performed for confirmation [33]. Alternative 99mTc bone scintigraphy or whole-body MRI may be considered for staging in cases F<sup>18</sup> FDG-PET is unavailable [3].

### Clonal and benign neoplastic conditions

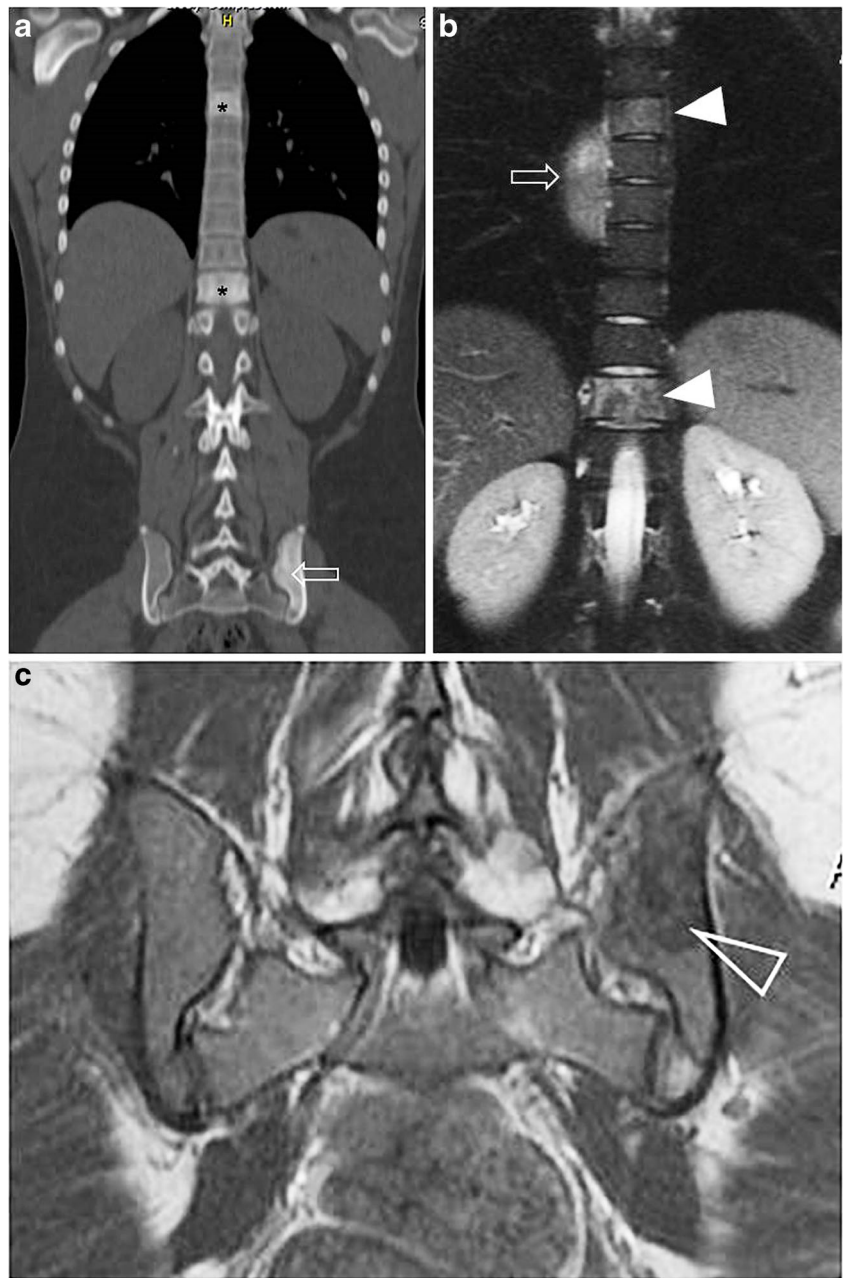
#### Langerhans cell histiocytosis

Langerhans cell histiocytosis is a clonal, single or multisystem disease, characterized by proliferation of Langerhans cells, affecting more often children between 1 and 5 years of age.

The skeleton is the most common site of involvement (60–80% of Langerhans cell histiocytosis cases), primarily in older children and adolescents. Skeletal lesions can be asymptomatic incidentalomas. Symptoms include pain, swelling, tenderness and systemic features like fever and malaise [34, 35].



**Fig. 11** A 16-year old girl diagnosed with mediastinal lymphoma and osseous involvement. **a** Coronal CT image (bone window) during PET-CT shows ivory appearance of the Th5, Th11 and L3 vertebral bodies (\*) and of the left iliac bone (*arrow*). Differential diagnosis for an ivory (sclerotic) bone includes chronic osteomyelitis, chronic recurrent multifocal osteomyelitis, osteosarcoma, osteoblastoma and metastatic disease due to neuroblastoma, medulloblastoma, osteosarcoma and Ewing sarcoma. **b** Coronal short tau inversion recovery MRI (TR/TE/TI: 3,500/43/150 ms). Notice the increased signal intensity of the bone marrow corresponding to sclerotic vertebral bodies (*arrowheads*) and part of a nodal mass at the posterior mediastinum (*arrow*). **c** Coronal T1-weighted MRI (TR/TE: 500/11 ms). Hypointense lesion is sharply delineated due to lymphomatous involvement (*arrowhead*)



Langerhans cell histiocytosis is a great mimicker of other entities. Radiographic appearances vary from purely lytic well-defined lesions with sclerotic margins to expansile lesions with endosteal scalloping or cortical disruption and associated aggressive periosteal reaction and soft-tissue mass. On MRI, lesions exhibit non-specific hypointensity on T1-W, hyperintensity on STIR sequences and variable contrast enhancement. Aggressive lesions are associated with perilesional edema. Involuting lesions may exhibit sclerosis and high signal intensity on T1-W images. Extensive bone marrow changes and/or a “budding appearance” due to endosteal scalloping or lesions with mixed aggressive and benign characteristics are suggestive of Langerhans cell histiocytosis [35]. Practically, Langerhans cell histiocytosis should

always be considered in the differential diagnosis of multifocal marrow lesions in children (Fig. 14). MRI may demonstrate asymptomatic bone marrow abnormalities earlier in the disease process, it identifies more skeletal lesions than plain radiography and bone scintigraphy and it also detects extraskelatal Langerhans cell histiocytosis lesions [36].

### Hereditary multiple osteochondromas

Hereditary multiple osteochondromas, also called hereditary multiple exostoses or hereditary osteochondromatosis or diaphyseal aclasis, is an autosomal dominant condition, characterized by multiple osteochondromas: benign sessile or pedunculated cartilage-



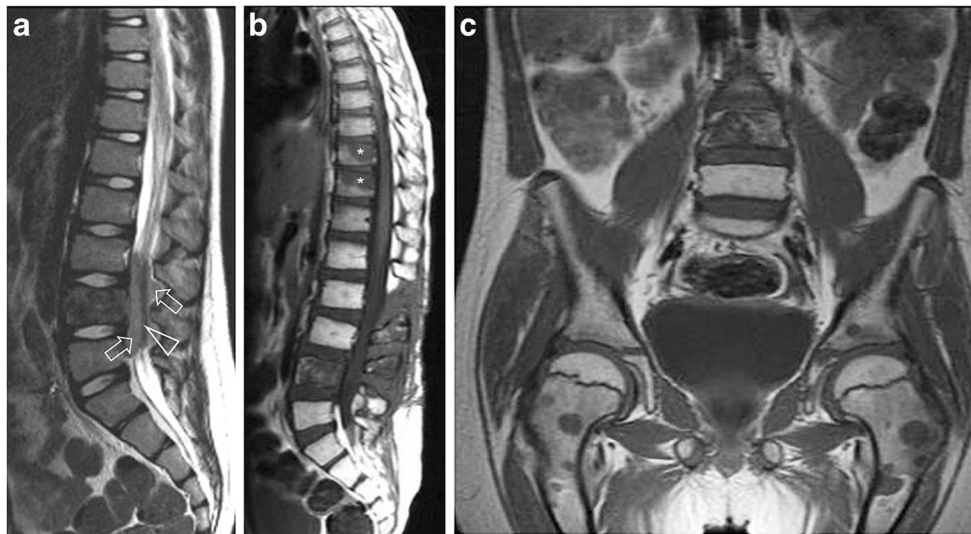


**Fig. 12** A 10-year-old boy with biopsy-proven osteosarcoma. **a** Sagittal T2-weighted MRI (TR/TE: 3,300/120 ms) at diagnosis. There is an expansile and profoundly hypointense mass at L4 associated with an epidural mass (*arrows*). Cauda equina (*arrowhead*) is seen as a thick stripe of crowded hypointense roots with effacement of cerebral spinal fluid high signal at this level. **b** Sagittal T1-weighted MRI (TR/TE: 500/11 ms) followed surgery, chemotherapy and radiotherapy. There are new

well-defined low-intensity lesions (\*). L4 contains a few areas of restored hyperintense fatty marrow. Note the depleted, diffusely hyperintense bone marrow from L2 downward, which corresponds to fatty transformation of marrow within the irradiated field. **c** Coronal T1-weighted MRI (TR/TE: 500/11 ms). There are hypointense sharply demarcated round lesions at the iliac and femoral bones

capped bone tumors that grow outward from the metaphyses of long bones or from flat bones (Fig. 15) [37]. Native cortical bone

extends into the stalk of the lesion, which can be thin or broad-based [38].

**Fig. 13** A 13-year-old boy with back pain and disseminated multifocal Ewing sarcoma at diagnosis. **a** Axial T1-weighted MRI (TR/TE: 500/11 ms) shows the well-defined hypointense lesions (*arrows*). **b** Axial post-gadolinium T1-weighted fat-saturated MRI (TR/TE: 650/12 ms) shows subtotal contrast enhancement (within circles). **c** Sagittal short tau inversion recovery MRI (TR/TE/TI: 3,500/43/150 ms) during follow-up shows multiple hyperintense vertebral lesions

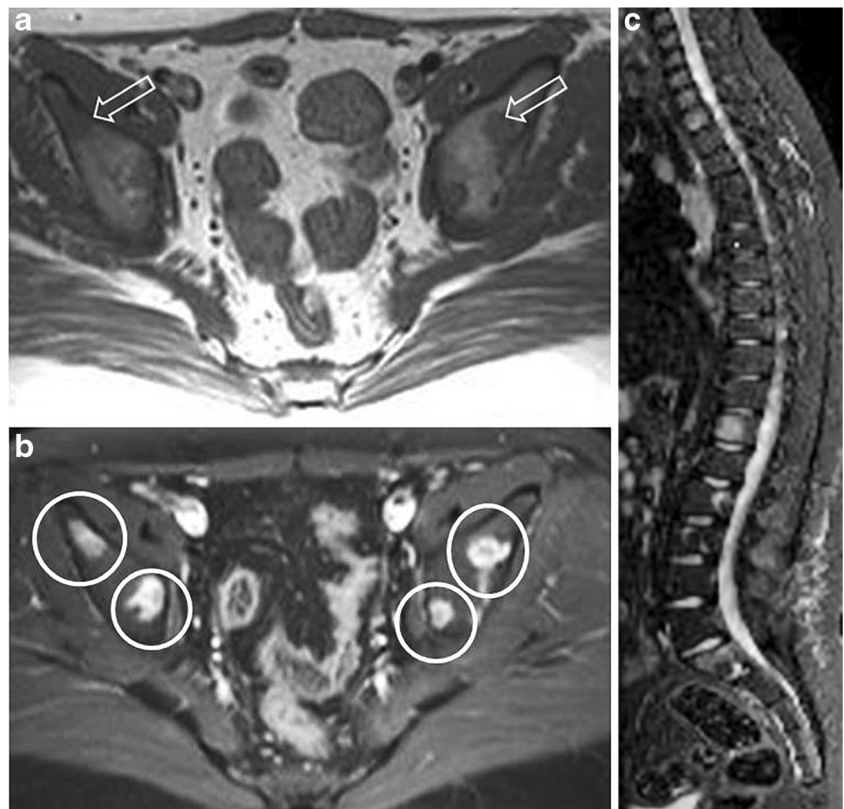
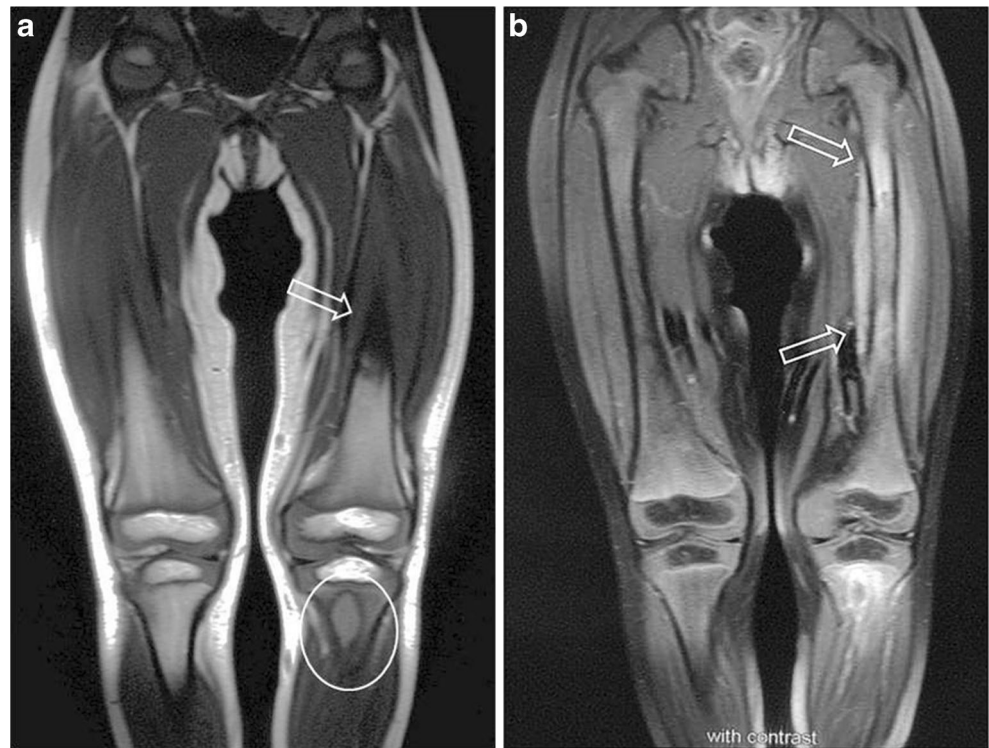


**Fig. 14** Langerhans cell Histiocytosis in a 5-year-old girl. Radiograph (not shown) demonstrates femoral periosteal reaction and a sharply demarcated lytic metaphyseal lesion with sclerotic margins at the left tibia. **a** Coronal T1-weighted MRI (TR/TE: 500/11 ms) shows femoral hypointensity (*arrow*) and a hyperintense compared to muscle metaphyseal lesion with a hypointense rim (*circle*). **b** Coronal post-gadolinium T1-weighted fat-saturated MRI (TR/TE: 650/12 ms) shows perilesional enhancement (*arrows*) and ring enhancement of the metaphyseal abnormality. Multiple lesions of different aggressiveness and the diaphyseal location were highly suggestive of Langerhan cell histiocytosis



The median age of diagnosis is 3 years. Nearly all affected individuals are diagnosed by 12 years of age [39].

Patients may be asymptomatic or significantly deformed by multiple large osteochondromas and symptomatic due to compression of muscles or neurovascular structures. Malignant transformation is more common in hereditary

multiple osteochondromas than in sporadic cases, with rates reported 0.5-25%. Radiologic and clinical features suggestive of malignant transformation are growth after skeletal maturity, newly seen radiolucency, flake-like calcifications, additional scintigraphic activity, cortical destruction, pain after puberty, soft-tissue mass and a thickened cartilage cap greater than 1.5-2 cm [40].



**Fig. 15** MRI of a 12-year-old girl with knee pain and osteochondromas on radiographs (not shown). **a** Sagittal T1-weighted MRI (TR/TE: 500/11 ms). There is a large sessile osteochondroma covered by a thickened cartilaginous cap (\*). Femoral cortex and bone marrow are in continuity with the lesion's cortex and bone marrow, respectively. **b** Coronal short

tau inversion recovery MRI (TR/TE/TI: 3,500/43/150 ms) of both knees. There are multiple thin, hyperintense cartilaginous caps (*open arrows*) over sessile exostoses. The pedunculated exostosis (*solid arrow*) grows outward and away from the joint

**Fig. 16** A 7-year-old boy with leg length discrepancy. Radiographs of the knee showed sharply defined lucent lesions, some surrounded by sclerosis, containing speckled matrix calcifications in the proximal tibia and fibula. **a** Sagittal T1-weighted MRI (TR/TE: 500/11 ms). Enchondromas appear as low-intensity front-like lesions at the distal femoral metaphysis and the proximal tibial metadiaphysis (*open arrows*), in continuity with epiphyseal cartilage (*middle black arrow*). **b** Sagittal T2 star gradient echo (TR/TE/FA: 1,040 ms/27 ms/30°). Enchondromas in the tibia and fibula (\*) exhibit the same signal intensity as hyaline cartilage and contain low intensity matrix calcifications (*arrowhead*)



MRI assesses cartilage thickness (and, consequently, possible malignant transformation), but more importantly edema indicative of a fracture in pedunculated lesions and the effect on adjacent structures for possible impingement [39, 40].

### Multiple enchondromatosis

Multiple enchondromatosis or Ollier disease, also referred to as dyschondroplasia or multiple cartilaginous enchondroses, is usually diagnosed during childhood and is a non-hereditary condition characterized by multiple intraosseous benign cartilaginous tumors. The estimated prevalence of the disease is 1 in 100,000 [37]. An asymmetrical distribution of cartilaginous lesions is observed, occasionally with subperiosteal extension (Fig. 16). Number, size and location of the enchondromas can be extremely variable. Enchondromas may cause skeletal deformities, limb length discrepancy, pain and the potential risk for malignant change to chondrosarcoma (20–50% of cases) [37, 41]. The condition in which multiple enchondromas is associated with hemangiomas is known as Maffucci syndrome.

### Polyostotic fibrous dysplasia

Polyostotic fibrous dysplasia represents the less frequent subtype of fibrous dysplasia, accounting for 20–30% of cases, and consists of a rare benign non-neoplastic skeletal developmental disorder

characterized by proliferation of medullary spaces by fibro-osseous tissue in multiple sites.

Polyostotic fibrous dysplasia presents earlier than the monostotic form. Mean age at presentation is 8 years; two-thirds of children become symptomatic by age 10 years. The condition is usually painless. Morbidity may arise from insufficiency fractures, deformities or compression/displacement of adjacent structures. Polyostotic fibrous dysplasia may involve large segments of bone and many or few bones, and often appears unilateral, showing a monomelic pattern.

Radiographic findings are extremely variable and consist of multiple mixed lytic/sclerotic areas. Lesions are largely isointense with areas of hypointensity on T1-W images and usually appear heterogeneously hyperintense on T2-W images (Figs. 17 and 18). Enhancement pattern is patchy, central, rim, homogeneous or a combination [42]. Characteristic appearances include shepherd's crook deformity (bowing deformity with varus angulation of the proximal femur), leontiasis ossea (marked deformities of frontal and facial bones resembling a lion's face) [43] and cherubism (polyostotic fibrous dysplasia of mandible and maxilla).

Associations include McCune-Albright syndrome (precocious puberty and café-au-lait spots), Mazabraud syndrome (polyostotic fibrous dysplasia associated with intramuscular myxomas; Fig. 18) and endocrinopathies (endocrinopathies include hypothalamic dysfunction, hyperprolactinemia, hyperthyroidism, Cushing disease and hypophosphatemia) [41, 42, 44].





**Fig 17** MRI of a 12-year-old boy with left femoral pain. **a** Coronal T1-weighted MR images (TR/TE: 500/11 ms) shows a hypointense area with sharply delineated sclerotic margins on the right (\*), an extensive hypointense lesion on the left with diaphyseal expansion and a possible fracture line (arrow). **b** Coronal short tau inversion recovery MRI (TR/TE/TI: 3,500/43/150 ms) demonstrates variably high signal intensity of

the lesions. The fracture line is visible (open arrow). Note the periosteal reaction at the mid diaphysis (solid arrow), cortical thinning and mild curved deformity at the left femur. Radiographs (not shown) confirm polyostotic large lytic and ground glass lesions with sclerotic margins at the pelvis, femora and tibiae, accompanied by endosteal scalloping, bowing and expansion of the left femur

**Infectious and inflammatory diseases**

**Multifocal osteomyelitis**

Osteomyelitis represents an inflammation of bone, occurs at any age and presents differently in infants and young children compared to older children and adolescents [45]. Osteomyelitis is usually due to the hematogenous spread of bacteria through the slow-flowing vascular sinusoids of the bloodstream into the bone, while inoculation following penetrating trauma or contiguous spread from neighboring infection is more common in older children and adults. Due to patent transphyseal vessels up to the age of 18 months, acute

hematogenous osteomyelitis affects the epiphyses in children younger than 2 years, which explains the higher prevalence of epiphyseal osteomyelitis, discitis and septic arthritis in infants and young children compared to older children [45]. Metaphyses and metaphyseal-equivalent sites of long bones and pelvis constitute the most vascularized part of bone and prevalent sites for hematogenous osteomyelitis [46].

Reduced immune responses in neonates and younger children account for the increased incidence of multifocal osteomyelitis and the milder clinical signs in younger age groups [45, 46].

Typical symptoms may be highly suggestive of the entity or unspecific, vague and include local pain and swelling,

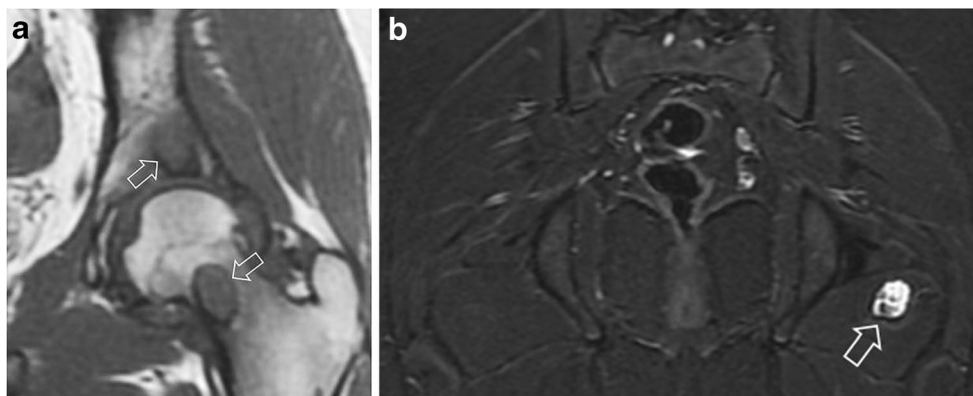


**Fig. 18** A 16-year-old girl with left hip pain and radiolucent lesions at radiographs. **a** Coronal T1-weighted MRI (TR/TE: 500/11 ms) shows fibrous areas of hypointensity and sharp sclerotic margins (arrow). **b** Coronal short tau inversion recovery MRI (TR/TE/TI: 3,500/43/

150 ms) shows a hyperintense well-defined lesion with a fatty suppressed hypointense rim (arrow). The combination of findings is consistent with soft-tissue myxoma and fibrous dysplasia (Mazabraud syndrome)

reduced range of motion, inability to bear weight and systemic symptoms: poor feeding, irritability, fever and general malaise [46, 47].

Multifocal osteomyelitis may occur as the result of simultaneous hematogenous spread of infection resulting in synchronous lesions. Osteomyelitis is considered subacute when lasting longer than 2 weeks and chronic when symptoms last longer than 6 weeks. Subacute and chronic lesions may present with mild symptoms. In this setting, initial scanning with a large field of view in small patients and whole-body MRI may exclude or identify silent foci however, MR detection of asymptomatic abnormalities in the contralateral extremity of children with a symptomatic limb and suspected osteomyelitis is not necessarily associated with altered patient management [48].

MRI is particularly useful for detecting and delineating the extent of bone, joint and soft-tissue lesions. Early osteomyelitis is seen as nonspecific ill-defined bone marrow edema (Fig. 19). Non-enhancing fluid collections as well as rim-enhancing abscesses may occur in the marrow, subperiosteal region or in the soft tissues and are depicted with MRI in detail [47]. Cartilaginous involvement is seen as areas of no enhancement in infants (Fig. 20) [45]. Joint involvement is seen as joint effusion, enhancing synovial capsule and reactive epiphyseal bone marrow edema. MRI findings may be nonspecific and should always be interpreted in conjunction with available radiographs and the patient's charts [46, 48, 49]. A wide zone of transition between diseased and normal marrow



**Fig. 19** A 1-year-old girl with irritability, tenderness on passive movement of legs and raised inflammatory markers. Coronal large field of view short tau inversion recovery MRI (TR/TE/TI: 3,500/43/150 ms) included the entire body area, pelvis and lower extremities to identify potential abnormal foci. There is a high-intensity lesion (arrow) at the right side of S1 corresponding to a metaphyseal-equivalent site. Blood cultures grew staphylococcus aureus treated effectively with antibiotics

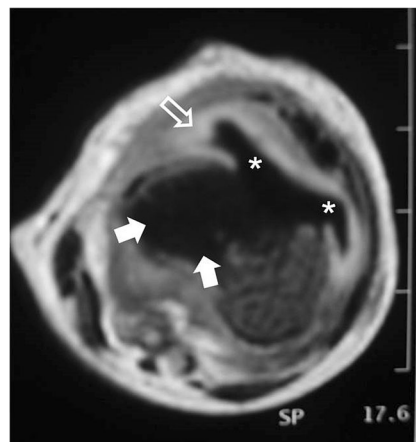


**Fig. 20** A neonate with left knee swelling, redness and focal tenderness that grew Group B streptococcus from aspirated pus. Axial post-gadolinium T1-weighted MRI (TR/TE: 650/12) shows thickening of hyperenhancing synovium (open arrow), joint effusion (\*) and a medial epiphyseal area that lacks enhancement (solid arrows) indicative of epiphyseal osteomyelitis and septic arthritis

on T1-W images is a feature favoring osteomyelitis over malignancy [50]. The presence of fat globules subperiosteally or within the infiltrating marrow process also is a sign of osteomyelitis and may be seen in the presence of diseased

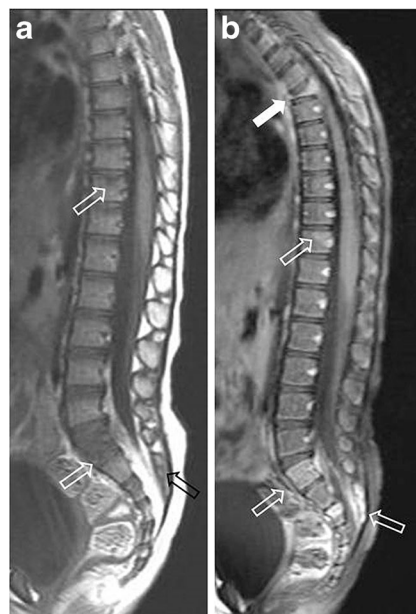


**Fig. 21** A 4-year-old girl with torticollis and lumbar pain had biopsy-proven chronic osteomyelitis treated with antibiotics. **a** Sagittal T1-weighted MRI (TR/TE: 500/11 ms). There are multiple low-intensity lesions (arrows). Note the wide zone of transition between the low-intensity lesion at Th11 and adjacent normal hyperintense yellow marrow. Lesions were more conspicuous at short tau inversion recovery sequences as areas of hyperintensity (not shown). **b** Sagittal post-gadolinium T1-weighted MRI (TR/TE: 650/12 ms). Lesions exhibit contrast enhancement (open arrows) without associated soft-tissue masses. Note insufficiency fracture at Th5 (solid arrow). Radiographic and CT appearances of S1 were compatible with an ivory vertebra carrying a wide differential diagnosis



**Fig. 22** A 20-year-old man with known chronic recurrent multifocal osteomyelitis and recurrent episodes of knee pain responding to non-steroidal anti-inflammatory agents. Coronal short tau inversion recovery MRI (TR/TE/TI: 3,500/43/150 ms) shows fluid collections subperiosteally (*arrows*) and epiphyseal/metaphyseal osteitis seen as hyperintense bone marrow (\*). Radiographs had shown symmetrical involvement of tibiae with widening and sclerosis indicative of chronic changes

converted fatty marrow and therefore is detected only in older children, adolescents and adults [50, 51]. Intravenous contrast

agent is essential when imaging infection to delineate avascular areas that may need drainage, to exclude intraspinal extension in spondylodiscitis and to increase confidence for the diagnosis; however, it has no value when conventional sequences are negative [52].

A Brodie abscess with the rim sign is the hallmark of sub-acute osteomyelitis whereas in chronic osteomyelitis MR appearances may be confusing with cortical/periosteal thickening and enhancing granulation tissue. Identification of an abscess, sequestrum, sinus tract and correlation with a sclerotic pattern on radiographs or CT may suggest the diagnosis [47]. Osteomyelitis mimics many benign and malignant entities and occasionally bone biopsy and cultures are requested for appropriate diagnosis (Fig. 21).

**Chronic recurrent multifocal osteomyelitis**

Chronic recurrent multifocal osteomyelitis (CRMO) is an idiopathic non-pyogenic inflammatory disorder occurring primarily in children and adolescents (mean age: 10 years) with various manifestations. A subtype called SAPHO (Synovitis, Acne, Pustulosis, Hyperostosis, Osteitis) is rare in children.

Onset of CRMO is usually insidious, characterized mostly by pain, tenderness, swelling and decreased range of movement, while systemic symptoms such as fever, weight loss and

**Fig. 23** MR imaging of a 16-year-old girl with acne, osteitis and chronic recurrent multifocal osteomyelitis in indicative locations. **a-c** Multilevel short tau inversion recovery MRI (TR/TE/TI: 3,500/43/150 ms) at various body areas. There are multiple lesions exhibiting increased signal intensity consistent with bone marrow edema, involving both clavicles, sternum, numerous vertebral bodies and the pelvic bones at various sites (within circles). **d** Axial T1-weighted MRI (TR/TE: 500/11 ms) at coronal levels corresponds to (a). The lesion is notably ill-defined and barely hypointense (*arrow*)

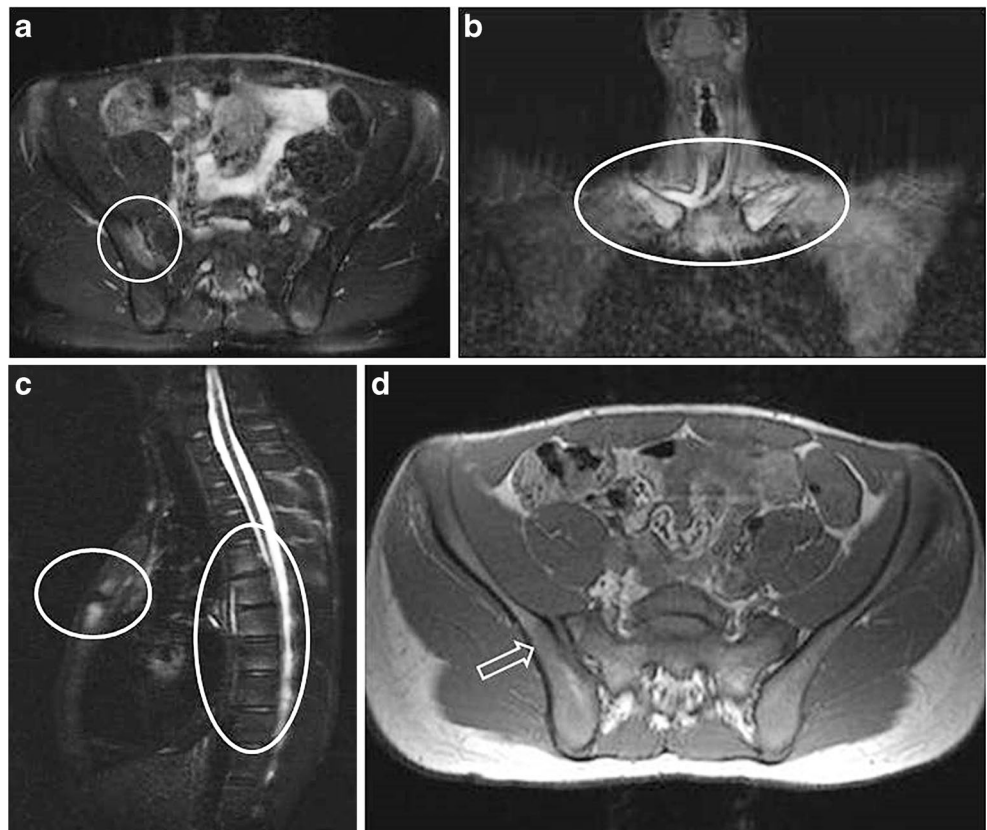






**Fig. 24** MRI of an overtrained 13-year-old female high jump athlete presenting with pain and reduced performances. Coronal short tau inversion recovery MRI (TR/TE/TI: 3,500/43/150 ms) shows two metaphyseal hyperintense ill-defined areas consistent with bone marrow edema, surrounding two hypointense stress fracture lines (*arrows*). Also note ill-defined epiphyseal bone marrow edema indicative of a stress reaction and periosteal reaction around the distal stress fracture

lethargy are less common. The disease may last from days to several years in a remittent way.

Multifocal lesions that are metaphyseal or mixed epiphyseal/metaphyseal, adjacent to a growth plate of a long bone in the lower extremities, are highly suggestive of CRMO in the appropriate clinical setting (Fig. 22). Other sites of involvement are the spine, pelvis with a predilection around the triradiate cartilage, ribs and sternum. CRMO is unique in its tendency to involve the clavicle, unlike hematogenous osteomyelitis, while symmetrical involvement, bilaterality and multifocality are usually present (Figs. 22 and 23) [53]. The spectrum of osteitis ranges from bone marrow edema undetectable on radiographs to lytic destruction and progressive sclerosis. MRI (especially whole-body MRI) is particularly useful for the diagnosis

because identification of asymptomatic lytic or sclerotic lesions, either unifocal or multifocal, helps to establish major criteria in a child with a normal cell blood count [53, 54]. CRMO is primarily a diagnosis of exclusion and bone marrow or targeted biopsy may be performed in selected cases.

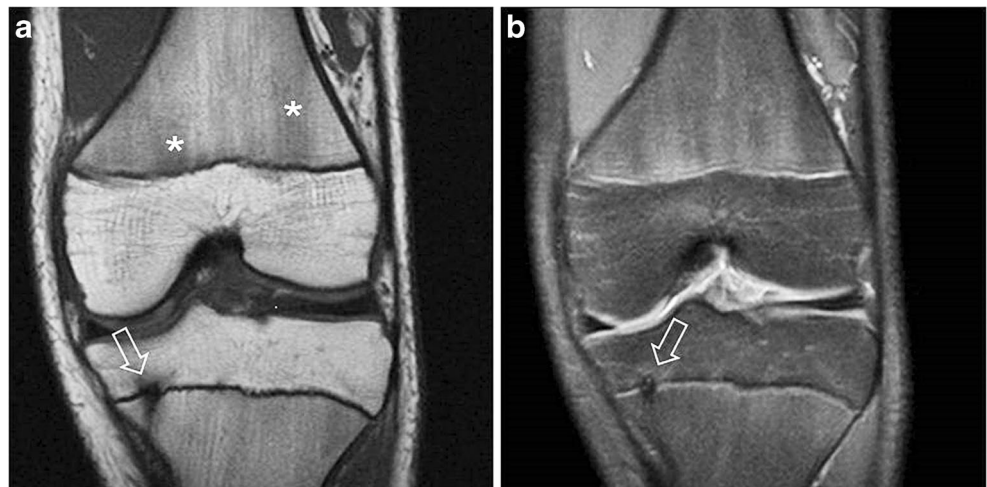
## Traumatic injuries

### Multiple stress fractures/reactions

Stress (overuse or fatigue) injuries range from stress reactions to stress fractures and occur when a normal bone is injured by abnormal repetitive activity [55]. Stress injuries may be multifocal depending on athletic activities. Radiographically, they may be occult or they may elicit a periosteal reaction and a radiopaque line/stripe perpendicular to supporting trabeculae when diaphyseal. Callus in short bones is the only radiographic abnormality present after the tenth day of symptoms [56, 57]. MRI shows bone marrow edema, occasionally surrounding a hypointense fracture line, both of which are oriented perpendicular to the supporting trabeculae of the bone (Fig. 24) [57]. Focal periphyseal edema in adolescents is considered related to early stages of physiological physal closure and may justify pain particularly when no other MRI abnormalities are present (Fig. 25) [58]. Differentiation of focal periphyseal edema lesions from early CRMO is difficult since both entities affect the bone marrow around the growth plate; focal periphyseal edema tends to be relatively limited and is associated with mild growth plate closure as well as spontaneous clinical and imaging resolution following restriction of physical activity. In the presence of large areas of periphyseal bone marrow abnormal signal, hematological malignancy should also be actively excluded.

Insufficiency fractures occur following normal mechanical stress on weakened bones. Such pathological fractures may

**Fig. 25** Focal periphyseal edema in a 13-year-old male jumper with knee pain relieved by rest. **a** Coronal T1-weighted MRI (TR/TE: 500/11 ms) shows a small area of growth plate fusion (*open arrow*). Also note flame-shaped, ill-defined, graded hypointense metaphyseal areas of prominent red marrow (\*). **b** Corresponding coronal short tau inversion recovery MRI (TR/TE/TI: 3,500/43/150 ms). There is periphyseal ill-defined perilesional bone marrow edema, seen as restricted areas of hyperintensity (*arrow*)



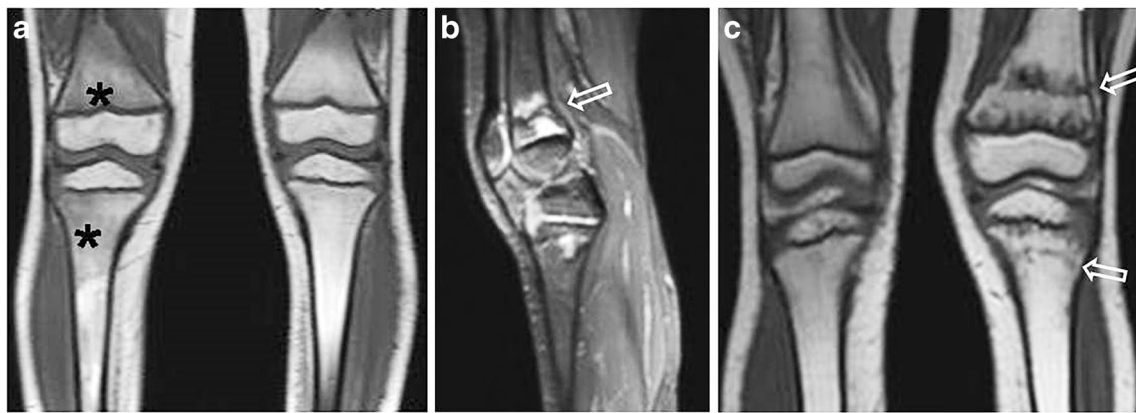


**Fig. 26** Serial MRI scans of a 5-year-old girl with an excised rhabdomyosarcoma from the left gastrocnemius muscle, post chemotherapy and radiotherapy. **a** Coronal T1-weighted MRI (TR/TE: 500/11 ms) of both knees. Normal prominence of red marrow on the right (\*). There is depleted bone marrow on the left seen as homogeneously hyperintense marrow. **b** Sagittal short tau inversion recovery MRI (TR/TE/TI: 3,500/43/150 ms) 1 year later during intense physiotherapy shows

a hypointense fracture line (*arrow*) while the remaining hyperintense metaphyseal areas have grown away from the growth plate. **c** Coronal T1-weighted MRI (TR/TE: 500/11 ms) through both knees 1 year later shows horizontal hypointense stippled lines (*arrows*) similar to growth arrest lines, probably representing sclerotic areas in the position of previous marrow involvement

occur following radiotherapy (Fig. 26), in children with leukemia in remission and in conditions predisposing to fractures such as osteogenesis imperfecta, x-linked hypophosphatemia, rickets, renal osteodystrophy and osteopetrosis.

Attention should be paid not to miss even a single fracture related to abuse in children, especially when younger than 2 years of age.

**Ischemia**

Avascular or aseptic necrosis, osteonecrosis and osteochondritis dissecans are terms used to describe the in situ death of cellular elements of bone. The terms aseptic (no

infection) and avascular necrosis (refers to pathogenesis) are alternative terms for epiphyseal osteonecrosis. Bone infarction is an alternative term for non-epiphyseal osteonecrosis. Early marrow changes (marrow ischemia) may be asymptomatic.

Foci of necrotic bone can be multiple, especially in children with predisposing factors: corticosteroid exposure, sickle cell disease, hemophilia, hyperbaric events, storage disorders, marrow infiltrating diseases, inflammatory bowel disease and inflammatory arthritis [59, 60]. Marrow ischemia can be detected with MRI as early as 6–12 h and appears as peripherally enhancing areas of marrow edema. Infarcts are characterized by a serpiginous, low intensity signal on T1-W sequence, surrounding an area of edematous, fatty or fibrous

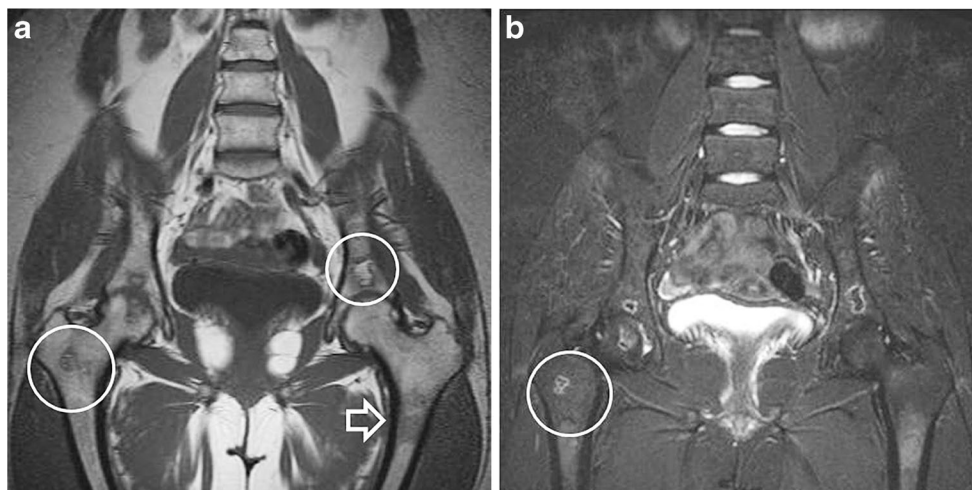


**Fig. 27** MRI of the pelvis in a 16-year-old girl with right hip pain and a known history of acute lymphoblastic leukemia. **a** Coronal T1-weighted MRI (TR/TE: 500/11 ms) shows multiple randomly distributed focal lesions (*within circles*) with a serpiginous low intensity rim and a high intensity center. Note a large area of bone marrow hyperplasia (*arrow*). **b**

Corresponding coronal short tau inversion recovery MRI (TR/TE/TI: 3,500/43/150 ms) demonstrates infarcts (*within circle*) exhibiting a high intensity rim and a fatty low intensity center. Imaging findings are characteristic of bone infarcts following corticosteroid therapy



**Fig. 28** A 4-year-old boy with bilateral hip pain and asynchronous changes of Perthes disease on radiographs. Coronal T1-weighted MRI (TR/TE: 500/11 ms) shows femoral head flattening, more prominent on the right, low signal intensity at both femoral heads and right metaphysis as well as a metaphyseal subchondral cyst (*arrow*). There is also right-side congruity loss with subluxation

bone marrow, depending on the stage of necrosis with or without collapsed bony segments (Fig. 27). The double layer sign consists of a hyperintense inner ring and a hypointense outer ring on non-fat-suppressed T2-W images and was thought to represent the reactive interface between ischemic and non-ischemic bone [60]. The “double line” sign is considered a chemical shift artifact and still a useful sign for the diagnosis of a necrotic area [61]. In sickle cell anemia patients, lesions with a bright marrow signal intensity on fat-suppressed T1-W images are consistent with hemorrhagic infarction. This hyperintensity favours infarction over infection.

Legg-Calvé-Perthes disease is an idiopathic avascular necrosis of the femoral heads, is bilateral in 10–20% of patients and usually affects children ages 4–8 years. When both hips are involved, they are usually affected successively, not simultaneously (Fig. 28).

Similarly, osteochondritis dissecans (osteochondral defect) is the final state of aseptic separation of an osteochondral fragment with gradual fragmentation of the articular surface and may successively affect multiple joints, usually the knees. The exact etiology remains unknown; however, in up to 40% of cases, patients disclose a history of trauma or repetitive injuries [62].

Clinical presentation of avascular necrosis varies from an asymptomatic state to significant pain, limping and disability requiring regular analgesia and physical therapy. Locking of joint suggests the presence of intra-articular loose bodies in osteochondritis dissecans.

### Take-home points

- MRI may detect a wide spectrum of benign and malignant conditions that result in nonspecific multifocal osseous or bone marrow lesions in children. Considering that imaging findings are interpreted based on age and available radiographic and clinical information, MRI may provide

a narrow differential diagnosis and determine appropriate patient management.

- Typical radiographic appearances prior to MRI are especially useful in polyostotic fibrous dysplasia, multiple osteochondromas, Ollier disease, osteosarcoma and Ewing sarcoma with skip lesions.
- Aggressive or widespread multifocal lesions have a differential diagnosis that includes metastatic disease, hematological malignancy, osteomyelitis, CRMO, Langerhans cell histiocytosis, Ewing sarcoma and osteosarcoma.
- A known history of malignancy, radiotherapy or intense athletic activity/physiotherapy warrants careful evaluation for metastases, bone marrow hyperplasia and stress/insufficiency injuries, respectively.
- Zone of transition: Ill-defined margins of lesions at T1-W sequences are in favor of benignity. Conversely, homogeneously hypointense lesions at T1-W sequences with a sharply defined margin without internal fatty rests are in favor of malignancy with the exception of fibrous dysplasia, bone infarcts and Langerhans cell histiocytosis that may exhibit hypointense sharp outer borders.
- The monomelic pattern is in favor of polyostotic fibrous dysplasia and stress injury.
- The location in the bone can be useful when considering that hematogenous metastases and infection have a predilection for metaphyses and metaphyseal-equivalent sites in children older than 2 years.

### Compliance with ethical standards

**Conflicts of interest** None

### References

1. Nievelstein RA, Littooi AS (2015) Whole-body MRI in paediatric oncology. *Radiol Med* 121:442–453
2. Goo HW (2015) Whole-body MRI in children: current imaging techniques and clinical applications. *Korean J Radiol* 16:973–985
3. Mentzel HJ, Kentouche K, Sauner D et al (2004) Comparison of whole-body STIR-MRI and 99mTc-methylene-diphosphonate scintigraphy in children with suspected multifocal bone lesions. *Eur Radiol* 14:2297–2302
4. Teixeira SR, Elias Junior J, Noqueira-Barbosa MH et al (2015) Whole-body magnetic resonance imaging in children: state of the art. *Radiol Bras* 48:111–120
5. Bley TA, Wieben O, Uhl M (2009) Diffusion-weighted MR imaging in musculoskeletal radiology: applications in trauma, tumors, and inflammation. *Magn Reson Imaging Clin N Am* 17:263–275
6. MacKenzie JD, Gonzalez L, Hernandez A et al (2007) Diffusion-weighted and diffusion tensor imaging for pediatric musculoskeletal disorders. *Pediatr Radiol* 37:781–788
7. Takahara T, Imai Y, Yamashita T et al (2004) Diffusion weighted whole body imaging with background body signal suppression



- (DWIBS): technical improvement using free breathing, STIR and high resolution 3D display. *Radiat Med* 22:275–282
8. Ording Müller LS, Avenarius D, Olsen OE (2011) High signal in bone marrow at diffusion-weighted imaging with body background suppression (DWIBS) in healthy children. *Pediatr Radiol* 41:221–226
  9. Costelloe CM, Madewell JE, Kundra V et al (2013) Conspicuity of bone metastases on fast Dixon-based multisequence whole-body MRI: clinical utility per sequence. *Magn Reson Imaging* 31:669–675
  10. Burdiles A, Babyn PS (2009) Pediatric bone marrow MR imaging. *Magn Reson Imaging Clin N Am* 17:391–409
  11. Waitches G, Zawin JK, Poznanski AK (1994) Sequence and rate of bone marrow conversion in the femora of children as seen on MR imaging: are accepted standards accurate? *AJR Am J Roentgenol* 162:1399–1406
  12. Taccone A, Oddone M, Dell'Acqua AD et al (1995) MRI “road-map” of normal age-related bone marrow. II. Thorax, pelvis and extremities. *Pediatr Radiol* 25:596–606
  13. Taccone A, Oddone M, Occhi M et al (1995) MRI “road-map” of normal age-related bone marrow. I. Cranial bone and spine. *Pediatr Radiol* 25:588–595
  14. Laor T, Jaramillo D (2009) MR imaging insights into skeletal maturation: what is normal? *Radiology* 250:28–38
  15. Orth RC, Guilleman P (2013) Skeletal manifestations of systemic disease. In: Caffey's pediatric diagnostic imaging, 12th edn. Coley BD (ed.). Elsevier Saunders pp 1543–1560
  16. Shabshin N, Schweitzer ME, Morrison WB et al (2006) High-signal T2 changes of the bone marrow of the foot and ankle in children: red marrow or traumatic changes? *Pediatr Radiol* 36:670–676
  17. Fletcher BD, Wall JE, Hanna SL (1993) Effect of hematopoietic growth factors on MR images of bone marrow in children undergoing chemotherapy. *Radiology* 189:745–751
  18. Chapman S, Nakielny R (2003) Aids to radiological differential diagnosis, 4th edn. Saunders: London
  19. Daldrup-Link HE, Franzius C, Link TM et al (2001) Whole-body MR imaging for detection of bone metastases in children and young adults: comparison with skeletal scintigraphy and FDG PET. *AJR Am J Roentgenol* 177:229–236
  20. Meyer JS, Siegel MJ, Farooqui SO et al (2005) Which MRI sequence of the spine best reveals bone-marrow metastases of neuroblastoma? *Pediatr Radiol* 35:778–785
  21. Riquelme V, García CB (2012) Imaging studies in early diagnosis of childhood leukemia. *Rev Chil Radiol* 18:24–29
  22. Sinigaglia R, Gigante C, Bisinella G et al (2008) Musculoskeletal manifestations in pediatric acute leukemia. *J Pediatr Orthop* 28:20–28
  23. Bohndorf K, Benz-Bohm G, Gross-Fengels W et al (1990) MRI of the knee region in leukemic children. Part I. Initial pattern in patients with untreated disease. *Pediatr Radiol* 20:179–183
  24. Kan JH, Hernanz-Schulman M, Frangoul HA et al (2008) MRI diagnosis of bone marrow relapse in children with ALL. *Pediatr Radiol* 38:76–81
  25. Guilleman RP, Voss SD, Parker BR (2011) Leukemia and lymphoma. *Radiol Clin N Am* 49:767–797
  26. Zhao XF, Young KH, Frank D et al (2007) Pediatric primary bone lymphoma-diffuse large B-cell lymphoma: morphologic and immunohistochemical characteristics of 10 cases. *Am J Clin Pathol* 127:47–54
  27. Mengiardi B, Honegger H, Hodler J et al (2005) Primary lymphoma of bone: MRI and CT characteristics during and after successful treatment. *AJR Am J Roentgenol* 184:185–192
  28. Kellenberger CJ, Miller SF, Khan M et al (2004) Initial experience with FSE STIR whole-body MR imaging for staging lymphoma in children. *Eur Radiol* 14:1829–1841
  29. Amstutz HC (1969) Multiple osteogenic sarcomata: metastatic or multicentric? Report of two cases and review of literature. *Cancer* 24:923–931
  30. Kunze B, Bürkle S, Kluba T (2009) Multifocal osteosarcoma in childhood. *Chir Organi Mov* 93:27–31
  31. Murphey MD, Senchak LT, Mambalam PK et al (2013) From the radiologic pathology archives: ewing sarcoma family of tumors: radiologic pathologic correlation. *Radiographics* 33:803–831
  32. Ladenstein R, Pötschger U, Le Deley MC et al (2010) Primary disseminated multifocal Ewing sarcoma: results of the Euro-EWING 99 trial. *J Clin Oncol* 28:3284–3291
  33. Newman EN, Jones RL, Hawkins DS (2013) An evaluation of [<sup>18</sup>F]-fluorodeoxy-D-glucose positron emission tomography, bone scan, and bone marrow aspiration/biopsy as staging investigations in Ewing sarcoma. *Pediatr Blood Cancer* 60:1113–1117
  34. Schmidt S, Eich G, Geoffroy A et al (2008) Extrasosseous langerhans cell histiocytosis in children. *Radiographics* 28:707–726
  35. Khung S, Budzik J-F, Amzallag-Bellenger E et al (2013) Skeletal involvement in Langerhans cell histiocytosis. *Insights Imaging* 4:569–579
  36. Goo HW, Yang DH, Ra YS et al (2006) Whole-body MRI of Langerhans cell histiocytosis: comparison with radiography and bone scintigraphy. *Pediatr Radiol* 36:1019–1031
  37. Pannier S, Legeai-Mallet L (2008) Hereditary multiple exostoses and enchondromatosis. *Best Pract Res Clin Rheumatol* 22:45–54
  38. Wuyts W, Schmale GA, Chansky HA et al (2000) Hereditary multiple osteochondromas. Gene Reviews [Internet], Seattle (WA). University of Washington, Seattle. Accessed 24 Oct 2016
  39. Murphey MD, Choi JJ, Kransdorf MJ et al (2000) Imaging of osteochondroma: variants and complications with radiologic pathologic correlation. *Radiographics* 20:1407–1434
  40. de Souza AM, Bispo Júnior RZ (2014) Osteochondroma: ignore or investigate? *Rev Bras Ortop* 49:555–564
  41. Muthusamy S, Conway SA, Temple HT (2014) Five polyostotic conditions that general orthopedic surgeons should recognize (or should not miss). *Orthop Clin N Am* 45:417–429
  42. Fitzpatrick KA, Taljanovic MS, Speer DR et al (2004) Imaging findings of fibrous dysplasia with histopathologic and intraoperative correlation. *AJR Am J Roentgenol* 182:1389–1398
  43. Maramattom BV (2006) Leontiasis ossea and post traumatic cervical cord contusion in polyostotic fibrous dysplasia. *Head Face Med* 2:24
  44. Cabral CE, Guedes P, Fonseca T et al (1998) Polyostotic fibrous dysplasia associated with intramuscular myxomas: Mazabraud's syndrome. *Skeletal Radiol* 27:278–282
  45. Offiah AC (2006) Acute osteomyelitis, septic arthritis and discitis: differences between neonates and older children. *Eur J Radiol* 60:221–232
  46. Jaramillo D (2011) Infection: musculoskeletal. *Pediatr Radiol* 41 Suppl 1:S127–S134
  47. Pugmire BS, Shailam R, Gee MS (2014) Role of MRI in the diagnosis and treatment of osteomyelitis in pediatric patients. *World J Radiol* 6:530–537
  48. Metwalli ZA, Kan JH, Munjal KA et al (2013) MRI of suspected lower extremity musculoskeletal infection in the pediatric patient: how useful is bilateral imaging? *AJR Am J Roentgenol* 201:427–432
  49. Collins MS, Schaar MM, Wenger DE et al (2005) T1-weighted MRI characteristics of pedal osteomyelitis. *AJR Am J Roentgenol* 185:386–393
  50. Henninger B, Glodny B, Rudisch A et al (2013) Ewing sarcoma versus osteomyelitis: differential diagnosis with magnetic resonance imaging. *Skeletal Radiol* 42:1097–1104
  51. Davies AM, Hughes DE, Grimer RJ (2005) Intramedullary and extramedullary fat globules on magnetic resonance imaging as a diagnostic sign for osteomyelitis. *Eur Radiol* 15:2194–2199

52. Averill LW, Hernandez A, Gonzalez L et al (2009) Diagnosis of osteomyelitis in children: utility of fat-suppressed contrast-enhanced MRI. *AJR Am J Roentgenol* 192:1232–1238
53. Khanna G, Sato TS, Ferguson P (2009) Imaging of chronic recurrent multifocal osteomyelitis. *Radiographics* 29:1159–1177
54. Von Kalle T, Heim N, Hospach T et al (2013) Typical patterns of bone involvement in whole-body MRI of patients with chronic recurrent multifocal osteomyelitis (CRMO). *Röfo* 185:655–661
55. Kerssemakers SP, Fotiadou AN, de Jonge MC et al (2009) Sport injuries in the paediatric and adolescent patient: a growing problem. *Pediatr Radiol* 39:471–484
56. Jaimes C, Jimenez M, Shabshin N et al (2012) Taking the stress out of evaluating stress injuries in children. *Radiographics* 32:537–555
57. Oestreich AE, Bhojwani N (2010) Stress fractures of ankle and wrist in childhood: nature and frequency. *Pediatr Radiol* 40:1387–1389
58. Zbojniec AM, Laor T (2011) Focal periphyseal edema (FOPE) zone on MRI of the adolescent knee: a potentially painful manifestation of physiologic physeal fusion? *AJR Am J Roentgenol* 197:998–1004
59. Kaste SC, Pei D, Cheng C et al (2015) Utility of early screening magnetic resonance imaging for extensive hip osteonecrosis treated with glucocorticoids. *J Clin Oncol* 33:610–615
60. Saini A, Saifuddin A (2004) MRI of osteonecrosis. *Clin Radiol* 59:1079–1093
61. Karantanas AH, Drakonaki EE (2011) The role of MR imaging in avascular necrosis of the femoral head. *Semin Musculoskelet Radiol* 15:281–300
62. Backes JR, Durbin TC, Bentley JC et al (2014) Multifocal juvenile osteochondritis dissecans of the knee: a case series. *J Pediatr* 34:453–458